主論文2

Short Contribution:

Comparisons of altimetry-derived geostrophic velocities and surface velocities determined from drifting buoy trajectory south of Japan

Kaoru Ichikawa

Department of Civil and Ocean Engineering, Faculty of Engineering, Ehime University, Matsuyama 790, Japan

Shiro Imawaki

Research Institute for Applied Mechanics, Kyushu University, Kasuga, Fukuoka 816, Japan

Haruo Ishii

Ocean Research Department, Japan Marine Science and Technology Center, Yokosuka, Kanagawa 237, Japan

Short title: SURFACE VELOCITIES DETERMINED FROM ALTIMETRY AND DRIFTER DATA

Abstract. Surface velocities determined from trajectory of a drifting buoy during March through November, 1987 are compared with surface geostrophic velocities determined from sea surface dynamic topography (SSDT) obtained from altimetry data with the aid of long-term hydrographic observations. In general, these velocities show similar temporal variations in both zonal and meridional components, except in a period when obvious error is found in the altimetric SSDT field. When the buoy was trapped by several meso-scale eddies, the comparison is especially good. Systematic discrepancy is found, however, when the buoy was in the Kuroshio region, because of using both temporally and spatially smoothed mean SSDT estimated from hydrographic observations; instead, surface geostrophic velocities determined from the altimetric SSDT referred to the improved geoid model result in better comparison.

1. Introduction

Satellite altimetry has been recognized as one of the most promising methods to observe variations of the velocity field in a wide area. It observes sea surface height over almost all the world oceans with reasonably high spatial resolution at short time intervals. The sea surface height is converted to the sea surface dynamic topography (hereinafter abbreviated as SSDT) by subtracting the geoid height; the SSDT is directly related to the oceanic surface pressure, and therefore the surface geostrophic velocity can be determined from it. In practice, however, only the temporal fluctuation part of the SSDT can be accurately determined since the available geoid model is not accurate enough to obtain the absolute SSDT.

In order to overcome this problem, two strategies to determine absolute SSDT are recently undertaken. One is to approximate the temporal mean SSDT lost in the analysis and to determine the approximated absolute SSDT by combining it with the fluctuation SSDT obtained from altimetry data. The mean SSDT can be estimated from the fluctuation SSDT alone in limited local areas of the western boundary current region (Tai, 1990; Qiu *et al.*, 1991), or is simply approximated by geopotential anomalies determined from hydrographic observations (Willebrand *et al.*, 1990; Stammer *et al.*, 1991; Ichikawa and Imawaki, 1992). The approximated absolute SSDT (hereinafter composite SSDT) is known to describe variations of oceanic conditions very well (*e.g.* Ichikawa and Imawaki, 1994). The other strategy to obtain the absolute SSDT is to improve geoid models. Apart from increasing observations of gravity field (Rapp and Wang, 1994; Paik *et al.*, 1988), geoid models can be improved by the combined use of altimetry data with gravity observations (Fukuda, 1990) or hydrographic observations (Glenn *et al.*, 1991; Imawaki *et al.*, 1991). If the geoid model is improved well, the absolute SSDT can be directly determined from altimetry data.

Temporal variations of the SSDT have been qualitatively evaluated by tide gauge records (*e.g.* Cheney *et al.*, 1989; Shibata and Kitamura, 1990) and by geopotential

anomalies determined from *in situ* hydrographic observations (*e.g.* Carton *et al.*, 1993; Imawaki *et al.*, 1995). However, these comparisons of temporal variations are limited in space since the time series of sea truth observations are required. Moreover, quantitative evaluations of the composite or absolute SSDT are not well studied. In addition, we need to verify the altimetry-derived surface velocity since the ultimate purpose of the use of altimetry data is determination of the surface velocity rather than SSDT itself. In order to determine the velocity vector, an extra procedure is required to convert along-track altimetry SSDT observations into a two-dimensional map of SSDT, and hence the accuracy of the altimetry-derived velocity would be decreased from that of SSDT itself. Only a few studies have been done for verification of the altimetry-derived velocity field (Willebrand *et al.*, 1990; Ebuchi and Hanawa, 1995).

In the present paper, we compare surface geostrophic velocities determined from the composite SSDT during the first year of Geosat Exact Repeat Mission (ERM) (Ichikawa and Imawaki, 1994) with surface velocities determined from trajectory of a drifting buoy in the area south of Japan. We also compare geostrophic velocities determined from the absolute SSDT using an improved geoid model (Ichikawa and Imawaki, 1995). The data and data-processing methods used in the the present analysis are explained in Section 2, while the results are described in Section 3 and discussed in Section 4. Finally in Section 5, concluding remarks are summarized.

2. Data and Method

We used Geosat altimetry data for the area southeast of Japan (20°– 45°N, 120°–150°E) during the first year of the ERM (from November 8, 1986 to November 17, 1987). Geosat altimetry data were distributed as the Geophysical Data Record by the National Oceanic and Atmospheric Administration (NOAA) (Cheney *et al.*, 1987). From the data, we produced time series of the absolute SSDT and the composite SSDT as follows; details of the methods are described in separated papers (Ichikawa and Imawaki, 1994;

1995). We applied the optimal interpolation in order to remove both the orbit error and noises in the data as well as to produce synoptic maps of the one-year mean elevation field and the 17-day averaged temporal fluctuation part of the SSDT around the mean (hereinafter abbreviated as the fluctuation SSDT), together with their estimated errors. The time series of the fluctuation SSDT field has been quantitatively verified by tide gauge records in the study area. The one-year mean elevation field is referred to the improved geoid model (Imawaki *et al.*, 1991) which is found to be accurate only in the local area south of Japan. Therefore the absolute SSDT is determined only in this local area by combining the fluctuation SSDT and the above-mentioned mean elevation field. On the other hand, the composite SSDT is everywhere determined by combining the fluctuation SSDT with the climatological mean SSDT. The climatological mean SSDT is determined from climatological mean geopotential anomalies at the sea surface relative to the 1000-dbar isobaric surface (on a $1° \times 1°$ grid). The anomalies were originally estimated from all the hydrographic data compiled since 1907 by the Japan Oceanographic Data Center, and smoothed over approximately 100 km in order to equalize the reliability of the data. The composite SSDT is determined at a grid $0.5° \times 0.5°$ for each 17-day cycle. Qualitatively, it has been evaluated by other *in situ* hydrographic observations and satellite infrared images.

The drifting buoy (# 1744) used in the present analysis was tracked by Argos system in the region south of Japan from 8 March (yearday 67) to 25 November (yearday 330), 1987. A drag with 1 m width and 4 m length was jointed to a float (0.9 m height) with a rope of 10 m length, so that its movement represents surface velocity at a depth of approximately 13 m. Since locations of the drifting buoy were irregularly sampled in time by NOAA satellites, observed meridional and zonal locations were regularized with two-hour interval by the spline interpolation; however, we did not interpolate locations when the observations were gapped for more than two days. Then 48-hour running mean of zonal and meridional locations was taken in order to remove the inertial and

tidal currents. Daily positions after those procedures are shown in Fig. 1. Fig. 1

At a position $\mathbf{r}_i$ for a day t_i, surface velocity $\mathbf{v}^{buoy}(\mathbf{r}_i, t_i)$ is calculated as follows;

$$\mathbf{v}^{buoy}(\mathbf{r}_i, t_i) = (\mathbf{r}_{i+\frac{1}{2}} - \mathbf{r}_{i-\frac{1}{2}})/(t_{i+\frac{1}{2}} - t_{i-\frac{1}{2}}).$$

On the other hand, geostrophic velocity $\mathbf{v}_p^{comp}(\mathbf{r}_i)$ at the position $\mathbf{r}_i$ can be determined from the composite SSDT field of the corresponding 17-day cycle p to which the date t_i belongs. Note that the latter velocity $\mathbf{v}_p^{comp}$ is 17-day averaged geostrophic velocity at the position $\mathbf{r}_i$, whereas the former is quasi-instantaneous daily-averaged surface velocity $\mathbf{v}^{buoy}$ at the position $\mathbf{r}_i$ and the day t_i. In order to make $\mathbf{v}^{buoy}$ consistent with the altimetry-derived velocity, we smoothed the time series of buoy-derived velocity $\mathbf{v}^{buoy}$; the smoothed velocity $\mathbf{v}_p^{buoy}(\mathbf{r}_i)$ for a position $\mathbf{r}_i$ and a cycle p to which time t_i belongs to is determined by

$$\begin{aligned} \mathbf{v}_p^{buoy}(\mathbf{r}_i) &= \gamma^{-1} \sum_{j=1}^{N} \exp\left(-(\mathbf{r}_i - \mathbf{x}_j)^2 / L^2\right) F_p(t_j)\, \mathbf{v}^{buoy}(\mathbf{x}_j, t_j) \\ \gamma &= \sum_{j=1}^{N} \exp\left(-(\mathbf{r}_i - \mathbf{x}_j)^2 / L^2\right) F_p(t_j) \end{aligned}$$

where N is the number of observations, $\mathbf{x}_j$ the horizontal position vector for j-th observation, L the decorrelation scale, and $F_p(t_i)$ the step function (0 or 1) which is 1 only when t_i belongs to the cycle p. Here we choose L as 50 km since the spatial resolution of the composite SSDT field is 0.5°. This smoothing would remove small scale phenomena both in space and time; some part of non-geostrophic velocities such as Ekman drift is expected to be removed by this operation. Hereinafter, we abbreviate the drifter-derived velocity $\mathbf{v}_p^{buoy}$ as $\mathbf{v}_b$, and the velocity $\mathbf{v}_p^{comp}$ determined from the composite SSDT as $\mathbf{v}_c$; similarly, the velocity determined from the absolute SSDT is denoted as $\mathbf{v}_a$.

3. Results

Surface velocities $\mathbf{v}_b$ at positions of the drifting buoy (Fig. 1) are determined from its trajectory. Surface geostrophic velocities $\mathbf{v}_c$ at the same positions are determined from the composite SSDT field. These two time series are plotted in Fig. 2; the statistics of the comparison between $\mathbf{v}_b$ and $\mathbf{v}_c$ are summarized in Table 1. As shown in the figure, these two velocities generally show similar temporal variations in both zonal and meridional components; correlation coefficients of 0.56 as zonal component and 0.48 as meridional component for 239 comparisons are significant for t-test of 99.9% confidence level.

Fig. 2

Tab. 1

The magnitude of difference of these velocities $|\mathbf{v}_b - \mathbf{v}_c|$ is plotted in Fig. 3 together with the magnitude of the drifter-derived surface velocity $|\mathbf{v}_b|$ and the estimated error of the altimetry-derived surface geostrophic velocity, which is determined from the estimated error of the fluctuation SSDT. In the figure, a systematic large velocity difference $|\mathbf{v}_b - \mathbf{v}_c|$ is found in the period of yeardays 250–280 when the magnitude of the velocity difference is much larger than the magnitude of the drifter-derived velocity $|\mathbf{v}_b|$ itself. Another large velocity difference $|\mathbf{v}_b - \mathbf{v}_c|$ is found in the period of yeardays 76–80 when the drifting buoy was located in the Kuroshio region (Fig. 1). Apart from these periods, the velocity difference does not exceed 0.3 m/s in general.

Fig. 3

Especially in the period of yeardays 120–210, the agreement between $\mathbf{v}_b$ and $\mathbf{v}_c$ is excellent (Fig. 2); correlation coefficients of zonal and meridional components are 0.70 and 0.82, respectively, and velocity difference is 0.1 m/s (Table 1). Therefore, during this period, we can expect to interpret the movement of the drifting buoy in the velocity field determined from the time series of the composite SSDT. Figure 4 shows synoptic maps of the composite SSDT together with the trajectory of drifting buoy. The drifting buoy was captured by a cyclonic eddy (indicated by "A" in the figure) centered at 27.5°N, 139°E on yearday 122 (panel (a)), and rotated around its center until about yearday 160 (panels (b)–(c)) while the center of the cyclonic eddy "A" moved westward.

Fig. 4

Then the buoy seems to have been captured into the anticyclonic eddy to the east of the drifting buoy (indicated by "W") which was approaching to the buoy. After rotating the center of "W", the buoy seems to have been separated from "W" in a period of yeardays 175–180 at approximately 28°N, 141°E, and was trapped into a large cyclonic eddy "B" which approached to the buoy from the east (panel (d)–(f)). These results indicate that the movement of the drifter is simply explained by propagation of the coherent flow pattern. When meso-scale eddies are coherently propagated, a buoy tends to be trapped in an approaching eddy and to be separated from an eddy going away. As a result of these successive captures by several eddies, the buoy moves eastward although no significant temporal mean current is present. Whether a drifting buoy trapped in an eddy continues its rotation around the eddy or is separated from the eddy would depend on the ratio of the time of propagation of the eddy for the length of its diameter $T_{prop} = 2R/c_p$ to the time of rotation around the eddy $T_{rot} = 2\pi R/U$, or $T_{prop}/T_{rot} = U/\pi c_p$, where R is the radius of the eddy, U the magnitude of velocity associated with the eddy, and c_p the magnitude of phase speed of the eddy. In the present case, the ratio is less than the unity (0.9) since U is about 0.2 m/s and c_p is about 0.07 m/s. This ratio smaller than the unity is somewhat consistent with the low Rossby number $U/\beta L^2$ ($\simeq$0.1) in this region, suggesting weaker advection in the vorticity balance.

The large velocity difference found in the period of yeardays 76–80 is considered to be originated from the small magnitude of velocities $\mathbf{v}_c$ determined from the composite SSDT (Fig. 2). In order to obtain the composite SSDT, the temporal fluctuation SSDT determined from the altimetry data is combined with the approximated one-year mean SSDT which is lost in the analysis of the altimetry data. In the present paper, the climatological mean SSDT estimated from hydrographic observations is used as the approximation of the one-year mean SSDT (Ichikawa and Imawaki, 1994); therefore the climatological mean geostrophic velocity used in the composite SSDT would be too small

compared with the one-year mean velocity of the Kuroshio. In addition to the difference of temporal averaging period, the former is decreased by low spatial resolution (1°× 1°) and spatial smoothing (approximately 100 km) of the climatological mean SSDT field. On the other hand, the geostrophic velocity $\mathbf{v}_a$ determined from the absolute SSDT can be obtained in this region south of Japan. Figure 5 shows the comparison of surface velocities determined from the drifting buoy trajectory $\mathbf{v}_b$, those from the composite SSDT $\mathbf{v}_c$ and those from the absolute SSDT $\mathbf{v}_a$ for the period of yeardays 67–90. As clearly seen in the figure, amplitude of variation of the surface geostrophic velocities $\mathbf{v}_a$ determined from the absolute SSDT is twice or three times larger than that of the geostrophic velocities $\mathbf{v}_c$ determined from the composite SSDT. The former velocities $\mathbf{v}_a$ are much closer to the drifter-derived surface velocities $\mathbf{v}_b$; the tilts (a) of the regression lines for comparison between $\mathbf{v}_b$ and $\mathbf{v}_c$, 0.10 and 0.41 (zonal and meridional components, respectively), are improved as 0.49 and 0.80 for comparison between $\mathbf{v}_b$ and $\mathbf{v}_a$. Note also that the magnitude of velocities calculated from horizontal gradients of SSDT assuming geostrophy tends to be decrease where the drifter rotates clockwise, since the Coriolis force would balance not only with the pressure gradient force but also with the centrifugal force. If we take the radius of the curvature of the flow as 250 km (Fig. 1) and the magnitude of the velocities as 1 m/s (Fig. 5), the estimated geostrophic velocities would be about 95 % of the actual velocity (Liu and Rossby, 1993).

Fig. 5

With the aid of the absolute SSDT, the separation of the drifting buoy from the Kuroshio is interpreted in the velocity field (Fig. 6). In the period of yeardays 66–82 (panel (a)), the absolute SSDT indicates that the drifting buoy was advected at the southern edge of the Kuroshio, although the absolute SSDT in the region 27°N–31°N and 133°E–135°E is contaminated by the error in the improved geoid model centered at 28°N, 133°E (Ichikawa and Imawaki, 1995). In the next period of yeardays 83–99 (panel (b)), the drifting buoy continued to flow at the southern edge of the Kuroshio at the first half of the period. But when the drifting buoy reached to the southern

Fig. 6

apex of the Kuroshio meander, it seems to have been captured into the western side of a cyclonic eddy centered at 28.5°N, 137.5°E, which approached to the Kuroshio large meander from the east; the ring was centered at 28°N, 138.5°E in the previous 17-day cycle (panel (a)). These results correspond to the class C warm outbreak discussed by Cornillon *et al.* (1986)

4. Discussion

The significant disagreement during yeardays 250–280 is originated from the large (0.6 m/s) meridional component of the altimetry-derived geostrophic velocity $\mathbf{v}_c$ (Fig. 2(b)), which seems to be too high for this region. The high velocity $\mathbf{v}_c$ is considered to be caused by an error in the fluctuation SSDT; note that the velocity difference is of the same magnitude of the estimated error in Fig 3. Since the altimetry data on most of descending orbits are missing during this period, small scale structures can not be smoothed out correctly because of insufficient altimetry data, as is indicated in the slightly larger estimated error than that of the first half of the year (Fig. 3). On the other hand, Fig. 3 indicates that the magnitude of the velocity observed by the drifting buoy is remarkably low; rms magnitude is 0.10 m/s in the period of yeardays 250–280. This weak velocity indicates that no significant variations existed in the SSDT field in this region. In other words, the ratio of the oceanic signal to the noise in the altimetry observations (S/N ratio) would be considerably low in this area. When the S/N ratio is lower than the provided one in the optimal interpolation used in the present analysis of the altimetry data, the estimated fluctuation SSDT field tends to include noises in the observations. We provided a uniform S/N ratio over the study area in the optimal interpolation since the estimated fluctuation SSDT field is not significantly sensitive to the choice of S/N ratio (Ichikawa and Imawaki, 1995), but the choice would be crucial for the velocity field calculated from the SSDT field since the spatial scale of the noises is small. More verifications of the fluctuation SSDT field in this region are necessary by

other observations together with several estimations of the fluctuation SSDT fields of different S/N ratio provided in the optimal interpolation.

Temporal resolution of 17-day of the composite SSDT is not fine enough to trace the drifting buoy in the altimetry-derived velocity field, since propagation of the coherent meso-scale patterns seems to be important. In order to increase temporal resolution without decreasing the spatial resolution, altimetry data sets from multiple satellites are necessary (Ichikawa and Imawaki, 1995). In addition, reconstruction of coherent structures through the decomposition of composite empirical orthogonal function analysis may be applied to "interpolate" temporal gap of 17 days.

In the region south of 23.5°N, the trajectory of the drifting buoy tends to loop (Fig. 1), indicating that the buoy was rotated over an eddy before leaving it and entering into another. This tendency would suggest that the local velocity associated with the eddy is much larger than the propagation speed of the eddy in this region. Eastward background current at 20–25°N indicated in the climatological mean geopotential anomalies may contribute to decrease westward propagation speed. However, more comparisons with trajectories of other drifting buoys are necessary to describe characteristics in each area to statistically remove possible effects of non-geostrophic currents in the buoy-derived velocity; results of comparisons with other drifting buoys will be reported in a separated paper.

5. Summary

From March through November, 1987, surface velocities at positions of a drifting buoy are determined from its trajectory, and are used to evaluate surface geostrophic velocities determined at the same positions from the composite SSDT field. These velocities show generally similar temporal variations in both zonal and meridional components; their correlation coefficients are 0.56 and 0.48, respectively.

Systematic discrepancy between these two velocities are found in a period of

yeardays 250–280. The discrepancy is caused by the error in the fluctuation SSDT field. Insufficiency of the altimetry data and the discrepancy of the S/N ratio assumed in the optimal interpolation may be the reasons of the error.

Another systematic discrepancy is found when the buoy was in the Kuroshio region south of Japan. In the region, the magnitude of surface geostrophic velocities determined from the composite SSDT is significantly smaller than that of the buoy-derived surface velocities, which is caused by substitution of spatially and temporally smoothed climatological mean SSDT for the one-year mean SSDT. Instead, the comparison to the drifter-derived velocities is much better for surface geostrophic velocities determined from the absolute SSDT referred to the geoid model improved by the combined use of Seasat altimetry data and contemporary *in situ* hydrographic observations; trends of regression lines for zonal and meridional components are 0.49 and 0.80, respectively.

Apart from these two periods, the difference between drifter-derived velocities and geostrophic velocities determined from the composite SSDT does not exceed 0.3 m/s in general. When the drifting buoy was trapped by several meso-scale eddies, the comparison is especially good. The movement of the buoy during such period is explained by the propagation of coherent flow structures; the drifter rotated around the center of an eddy, and then was captured into another eddy approaching to the buoy. As a result, the buoy moved eastward although no significant temporal mean current was present. This result is consistent with the low local Rossby number in this region.

Acknowledgments. We would like to thank Norihisa Imasato and colleagues of Department of Geophysics, Kyoto University for helpful overall discussions. Shigeru Aoki contributed to valuable discussions on interpretation of the results. Most of the study was completed when K.I. was at Kyoto University. The climatological mean geopotential anomalies for the western North Pacific were provided by the Japan Oceanographic Data Center. Data were processed on a FACOM computer at the Data Processing Center of Kyoto University. The figures were produced by GFD–DENNOU Library. This research was supported in

part by a Grant-in-Aid for Scientific Research from the Ministry of Education, Science, and Culture, Japan.

References

Carton, J.A., G.A. Chepurin, G.K. Korotaev and T. Zhu (1993): Comparison of dynamic height variations in the tropical Atlantic during 1987–1989 as viewed in sections hydrography and Geosat altimetry. *J. Geophys. Res.*, **98**(C8), 14369–14377.

Cheney, R.E., B.C. Douglas, R.W. Agreen, L. Miller, D.L. Porter, and N.S. Doyle (1987): *Geosat altimeter geophysical data record user handbook.* NOAA Tech. Memo. NOS NGS-46, U.S. Govt. Print. Office, Washington, D.C., 29 pp.

Cheney, R.E., B.C. Douglas and L. Miller (1989): Evaluation of Geosat altimeter data with application to tropical Pacific sea level variability. *J. Geophys. Res.*, **94**(C4), 4737–4747.

Cornillon P., D. Evans, and W. Large (1986): Warm outbreaks of the Gulf Stream into the Sargasso Sea. *J. Geophys. Res.*, **91**(C5), 6583–6596.

Ebuchi, N. and K. Hanawa (1995): Comparison of surface current variations observed by TOPEX altimeter with TOLEX–ADCP data. submitted to *J. Oceanogr.*

Fukuda, Y. (1990): Precise determination of local gravity field using both the satellite altimeter data and the surface gravity data. *Bull. of the Ocean Res. Inst.*, **28**, 133pp.

Glenn, S.M., D.L. Porter, and A.R. Robinson (1991): A synthetic geoid validation of Geosat mesoscale dynamic topography in the Gulf Stream region. *J. Geophys. Res.*, **96**(C4), 7145–7166.

Ichikawa, K. and S. Imawaki (1992): Fluctuation of sea surface dynamic topography southeast of Japan estimated from Seasat altimetry data. *J. Oceanogr.*, **48**, 155–177.

Ichikawa, K. and S. Imawaki (1994): Life history of a cyclonic ring detached from the Kuroshio Extension as seen by the Geosat altimeter. *J. Geophys. Res.*, **99**(C8), 15953–15966.

Ichikawa, K. and S. Imawaki (1995): Sea surface dynamic topography fluctuations southeast of Japan estimated from Geosat altimetry data. submitted to *J. Oceanogr.*.

Imawaki, S., K. Ichikawa and H. Nishigaki (1991): Mapping the mean sea surface elevation field from satellite altimetry data using optimal interpolation. *Marine Geodesy*, **15**, 31–46.

Imawaki, S., M. Gotoh, H. Yoritaka, N. Yoshioka and A. Misumi (1995): Detecting fluctuation of the Kuroshio axis south of Japan using TOPEX/POSEIDON altimeter data. submitted to *J. Oceanogr.*

Liu, M. and T. Rossby (1993): Observations of the velocity and vorticity structure of Gulf Stream meanders. *J. Phys. Oceanogr.*, **23**, 329–345.

Paik H.J., J.-S. Leung, S.H. Morgan and J. Parker (1988): Global gravity survey by an orbiting gravity gradiometer. *EOS*, **69**, 1601, 1610–1611.

Qiu, B., K.A. Kelly, and T.M. Joyce (1991): Mean flow and variability in the Kuroshio Extension from Geosat altimetry data. *J. Geophys. Res.*, **96**(C10), 18,491–18,501.

Rapp, R.H., and Y.M. Wang (1994): Dynamic topography estimates using Geosat data and a gravimetric geoid in the Gulf Stream region. *Geophys. J. Int.*, *117*, 511–528.

Shibata A. and Y. Kitamura (1990): Geosat sea level variability in the tropical Pacific in the period from November 1986 to February 1989, obtained by collinear method. *Oceanogr. Mag.*, **40**, 1–26.

Stammer, D., H.-H. Hinrichsen, and R.H. Käse (1991): Can meddies be detected by satellite altimetry? *J. Geophys. Res.*, **96**(C4), 7005–7014.

Tai, C.-K., and W.B. White (1990): Eddy variability in the Kuroshio Extension as revealed by Geosat altimetry: Energy propagation away from the jet, Reynolds stress, and seasonal cycle. *J. Phys. Oceanogr.*, *20*, 1761–1777.

Willebrand, J., R.H. Käse, D. Stammer, H.-H. Ninrichsen, and W. Karauss (1990): Verification of Geosat sea surface topography in the Gulf Stream Extension with surface drifting buoys and hydrographic measurements. *J. Geophys. Res.*, **95**(C3), 3007-3014.

This manuscript was prepared with the AGU LaTeX macros v3.1.

高度計データから求めた地衡流速と漂流ブイの軌跡から求めた表層流速の日本南方における比較

市川 香*, 今脇資郎†, 石井春雄‡

要旨

1987 年 3 月～11 月の漂流ブイの軌跡から求めた表層流速と、人工衛星海面高度計データと海洋観測データより近似的に得た合成海面力学高度から求めた地衡流速を比較した。一部の明らかな誤差を除き、東西・南北成分ともに全般に両者は似た時間変動を示した。特に、漂流ブイがいくつかの中規模渦に捕捉されていた期間では、両者は特に良く一致した。一方、ブイが黒潮域にあった場合には、系統的な差が見られた。これは、合成海面力学高度に使われている平均海面力学高度が時・空間的に平滑化されているためである。それに対して、この海域での改良ジオイド・モデルを基にした海面力学高度から求めた地衡流速は、ブイ流速と良く一致した。

*愛媛大学工学部土木海洋工学科 〒790–77 愛媛県松山市文京町 3

†九州大学応用力学研究所 〒816 福岡県春日市春日公園 6–1

‡海洋科学技術センター海洋研究部 〒237 神奈川県横須賀市夏島町 2–15

Fig. 1. Daily positions of a drifting buoy released south of Kyushu (marked by a cross) on yearday 67, 1987, and lost at 22.4°N, 144.2°E (marked by a star) on yearday 330, 1987; position data are missing during yeardays 205–209 around 25°N, 142°E.

Fig. 2. Time series of surface velocities determined from drifting buoy trajectory $\mathbf{v}_b$ (solid line), and from the composite SSDT $\mathbf{v}_c$ (broken line) for zonal component (a) and meridional component (b).

Fig. 3. Time series of the magnitude of velocity difference $|\mathbf{v}_b - \mathbf{v}_c|$ (solid line). The magnitude of the buoy-derived velocity $\mathbf{v}_b$ is also plotted by a thick dotted line, while the estimated error of the altimetry-derived geostrophic velocity $\mathbf{v}_c$ is shown by a thin dotted line.

Fig. 4. Synoptic maps of the composite SSDT during yearday 118 (a) to 219 (f) superimposed on daily positions of the drifting buoy. The observation period (yeardays) of each panel is indicated at the top. Beginning and ending positions of the drifting buoy trajectory in each period are indicated by a cross and a star, respectively. Contour interval is 0.05 m and shading interval is 0.1 m; the lower composite SSDT is shaded more heavily. Contours and shading are omitted at points where the estimated error of the fluctuation SSDT exceeds 0.16 m. Arrowheads indicate the direction of geostrophic velocities, and letters "A", "B" and "W" are drawn for the convenience of discussion.

Fig. 5. Time series of surface velocities determined from the drifting buoy trajectory $\mathbf{v}_b$ (solid line), from the composite SSDT $\mathbf{v}_c$ (broken line), and from the absolute SSDT $\mathbf{v}_a$ (dotted line) for zonal component (a) and meridional component (b) during the period of yeardays 67–90; the drifting buoy was in the Kuroshio region in this period.

Fig. 6. Same as Fig. 4 except for the period from yeardays 66 (a) to 99 (b) and for 0.1 m contour interval. Inside the dotted line, contemporary hydrographic observation data were used in the geoid model improvement.

Table 1. Statistics of the comparison of surface velocities determined from the composite SSDT $\mathbf{v}_c$ and those from the drifting buoy trajectory $\mathbf{v}_b$. They include the number of data (n) used in this comparison, root-mean-squared difference (VD), correlation coefficient (r), tilt (a) and bias (b) of regression line; $\mathbf{v}_c = a \times \mathbf{v}_b + b$; the unit of VD and b is m/s. Comparison is made for zonal (u-) and meridional (v-) components individually.

	n	VD	r	a	b
Total (67–321)					
u-comp.	239	0.14	0.56	0.52	0.01
v-comp.	239	0.20	0.48	1.20	0.08
Subtotal (67–90)					
u-comp.	21	0.25	0.22	0.10	0.16
v-comp.	21	0.27	0.94	0.41	-0.09
Subtotal (120–210)					
u-comp.	85	0.08	0.70	0.89	-0.01
v-comp.	85	0.09	0.82	0.74	-0.01

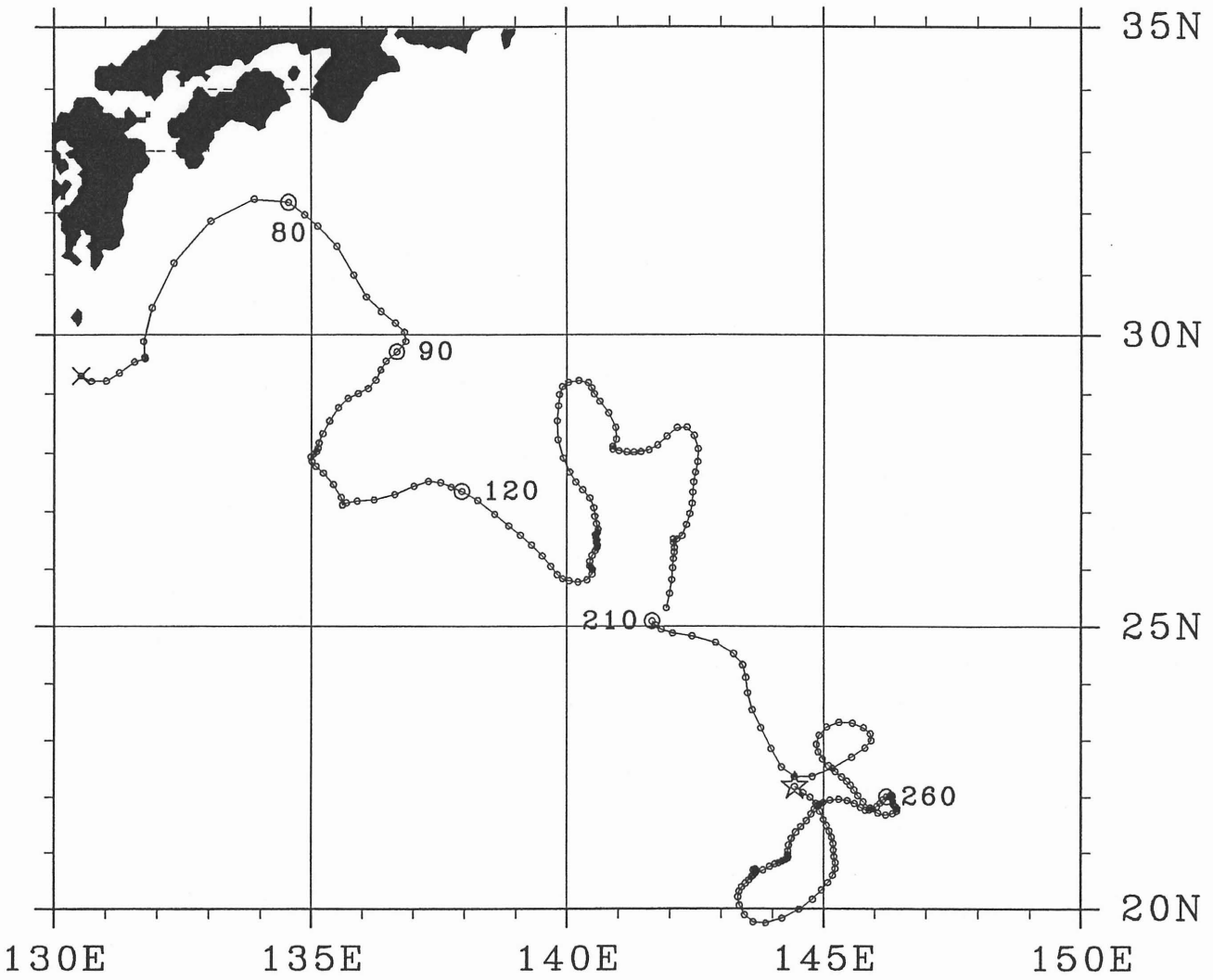

Fig1

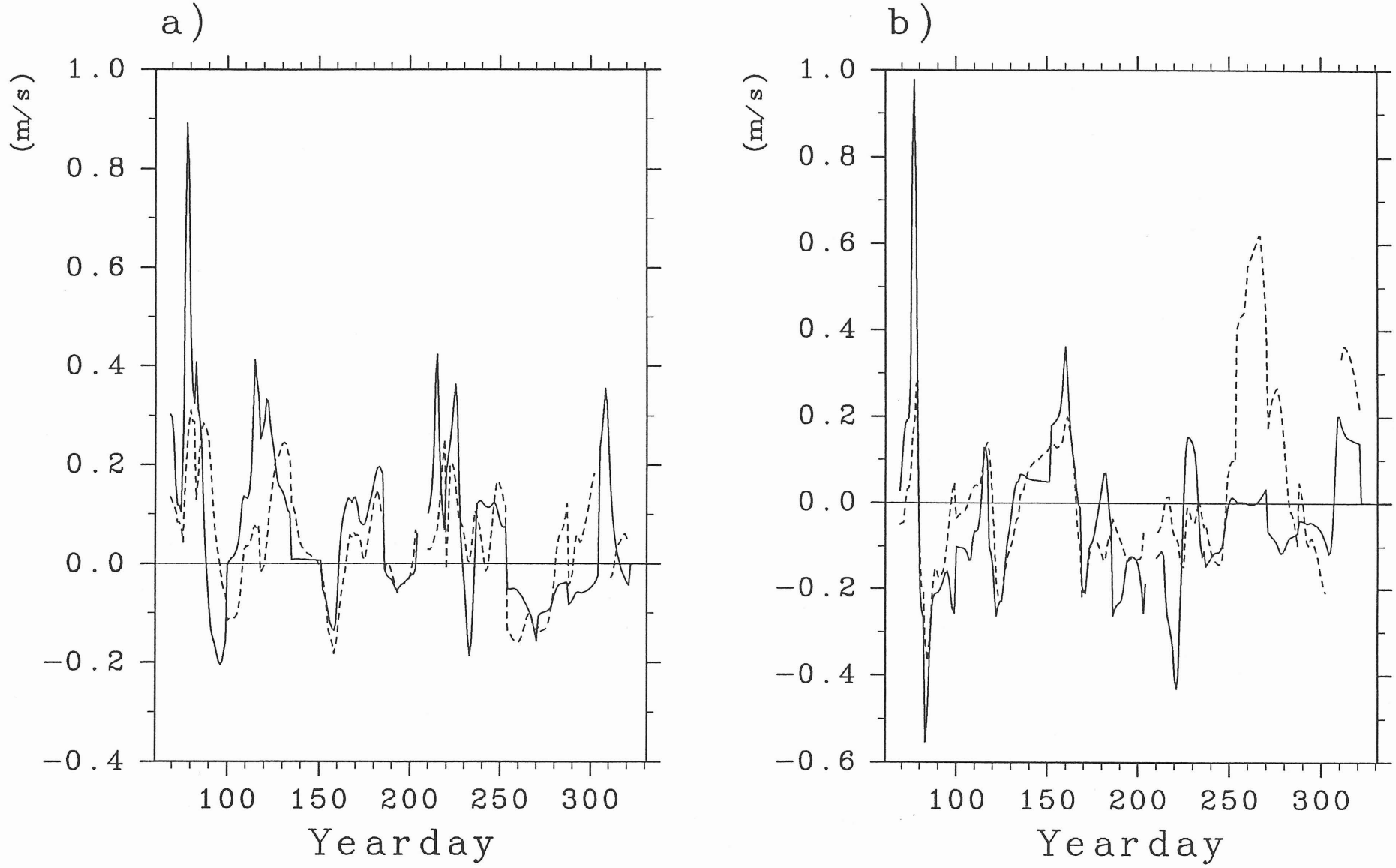

Fig 2

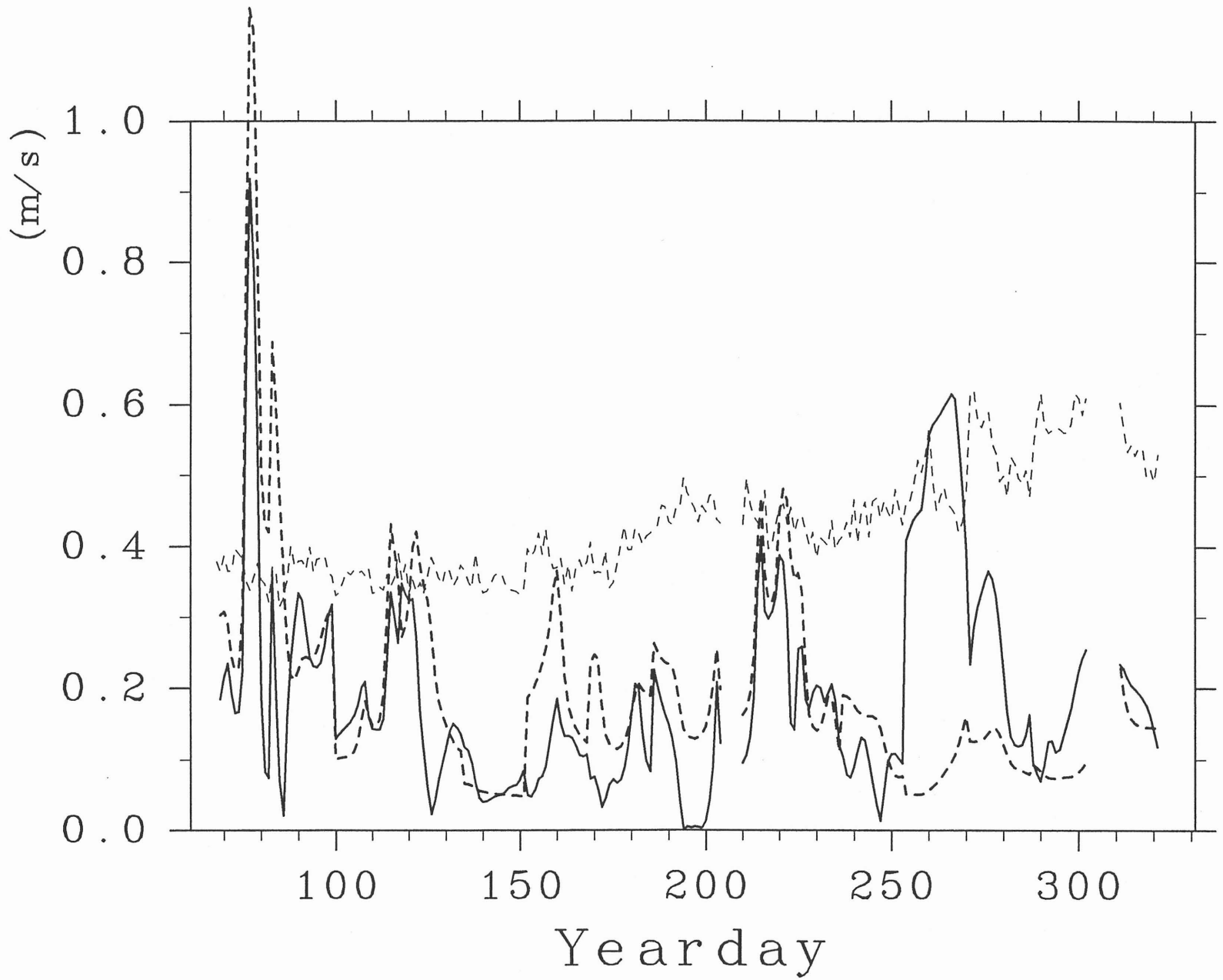

Fig 3

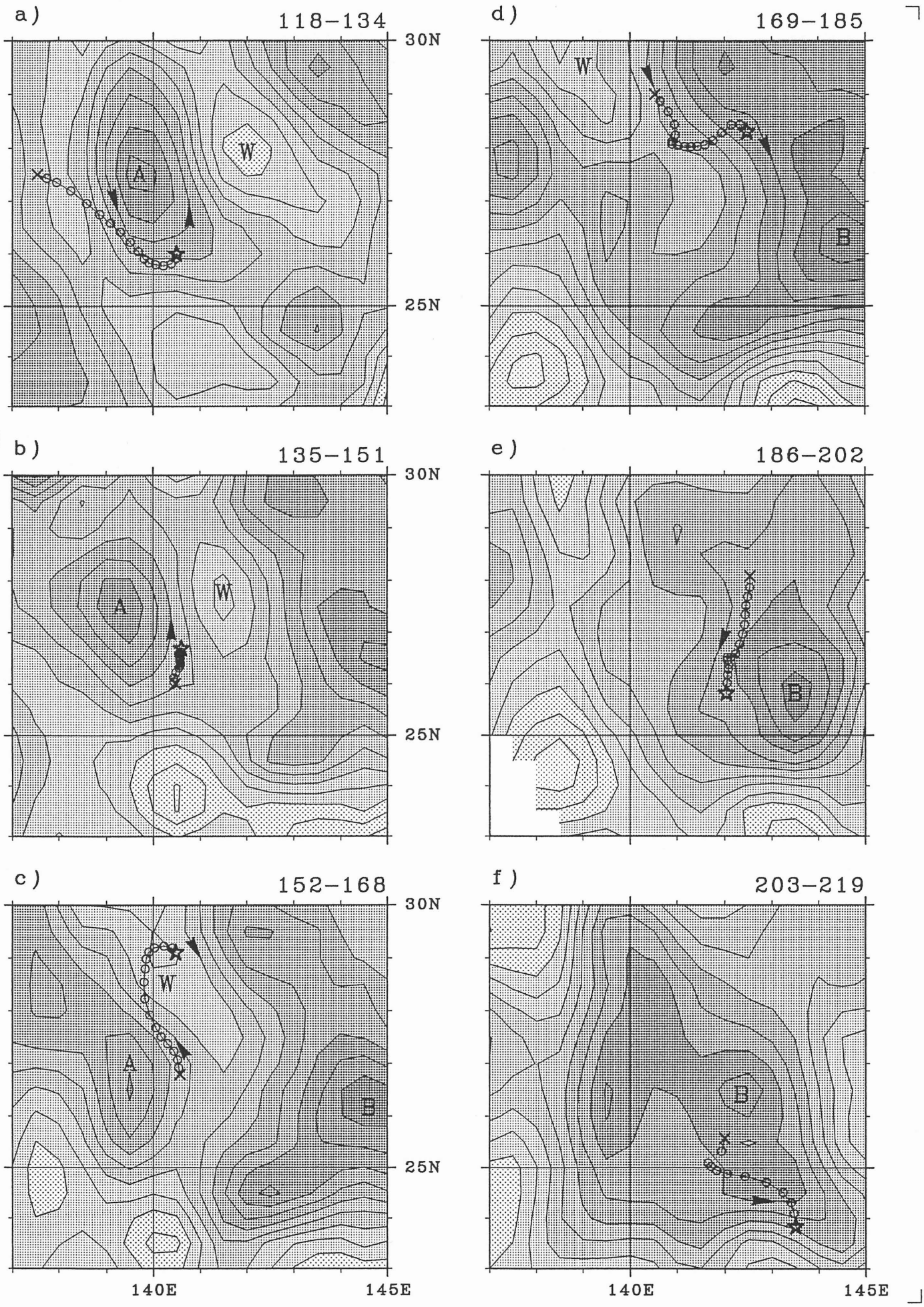
a)
118–134
30N
25N
W
A
b)
135–151
30N
25N
A
W
c)
152–168
30N
25N
W
A
B
140E
145E
d)
169–185
W
B
e)
186–202
B
f)
203–219
B
140E
145E

Fig 4

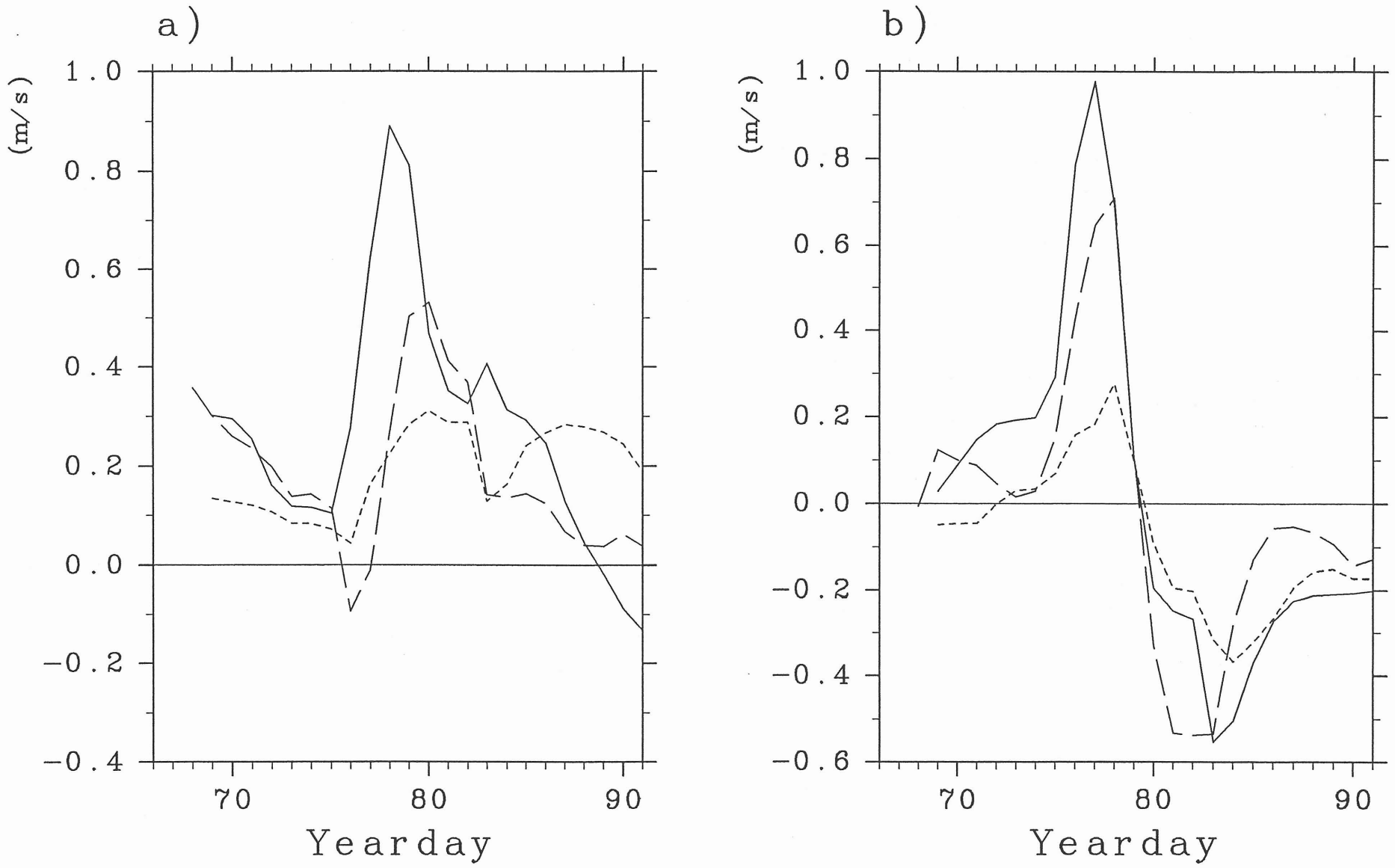

Figs

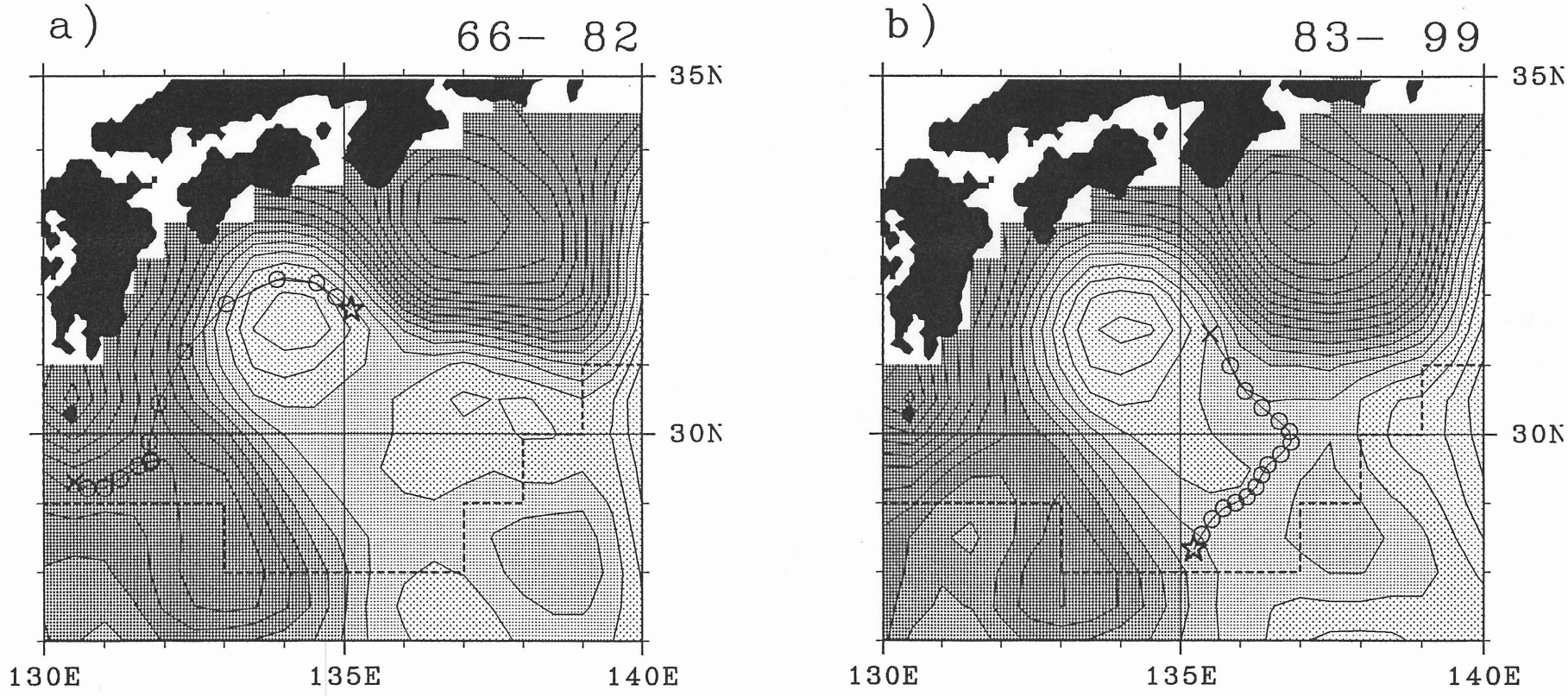

Fig 6